Journal of the Mechanics and Physics of Solids 73 (2014) 22–37

Contents lists available at ScienceDirect

Journal of the Mechanics and Physics of Solids

journal homepage: www.elsevier.com/locate/jmps

Designing nacre-like materials for simultaneous stiffness, strength and toughness: Optimum materials, composition, microstructure and size

Francois Barthelat

Department of Mechanical Engineering, McGill University, Montreal, QC, Canada

ARTICLE INFO

Article history:
Received 15 January 2014
Received in revised form
6 August 2014
Accepted 24 August 2014
Available online 6 September 2014

Keywords:
Nacre
Staggered composites
Biomimetics
Design optimization
Microstructure
Stiffness
Strength
Energy absorption
Toughness

ABSTRACT

Nacre, bone and spider silk are staggered composites where inclusions of high aspect ratio reinforce a softer matrix. Such staggered composites have emerged through natural selection as the best configuration to produce stiffness, strength and toughness simultaneously. As a result, these remarkable materials are increasingly serving as model for synthetic composites with unusual and attractive performance. While several models have been developed to predict basic properties for biological and bio-inspired staggered composites, the designer is still left to struggle with finding optimum parameters. Unresolved issues include choosing optimum properties for inclusions and matrix, and resolving the contradictory effects of certain design variables. Here we overcome these difficulties with a multi-objective optimization for simultaneous high stiffness, strength and energy absorption in staggered composites. Our optimization scheme includes material properties for inclusions and matrix as design variables. This process reveals new guidelines, for example the staggered microstructure is only advantageous if the tablets are at least five times stronger than the interfaces, and only if high volume concentrations of tablets are used. We finally compile the results into a step-by-step optimization procedure which can be applied for the design of any type of high-performance staggered composite and at any length scale. The procedure produces optimum designs which are consistent with the materials and microstructure of natural nacre, confirming that this natural material is indeed optimized for mechanical performance.

1. Introduction

High-performance biological materials such as bone, teeth, mollusk shells, arthropod shells or spider silk boast impressive mechanical properties which are currently unmatched by their engineering counterparts (Meyers et al., 2008). The keys to this performance are sophisticated microstructure organized over several hierarchical length scales, resulting in mechanisms which greatly "amplify" the properties of their relatively weak ingredients (Fratzl and Weinkamer, 2007; Ortiz and Boyce, 2008; Espinosa et al., 2009). The structure and mechanisms of these natural materials are therefore attracting an increasing amount of attention, and are also inspiring the development of novel biomimetic materials with superior performance (Espinosa et al., 2009; Mayer, 2005; Barthelat, 2007). In this area, nacre from mollusk shells has now

E-mail address: francois.barthelat@mcgill.ca

http://dx.doi.org/10.1016/j.jmps.2014.08.008
0022-5096/

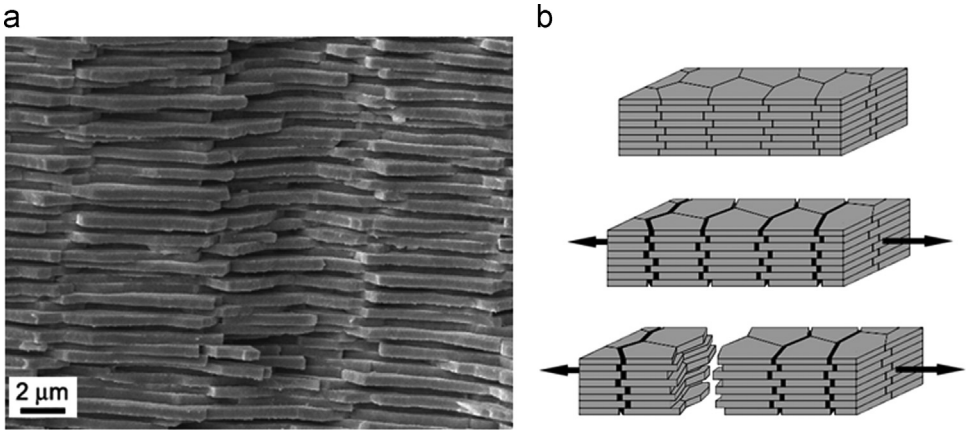

Fig. 1. (a) SEM image of nacre from *Trochus Niloticus* (Top shell); (b) schematic of the three-dimensional staggered structure of nacre with deformation and failure mechanism (adapted from (Barthelat et al., 2007)).

become the archetype of the natural "model" for bio-inspired hard materials. Nacre is a staggered composite made of microscopic mineral tablets with high aspect ratio, arranged in a three dimensional fashion. These microscopic bricks represent 95% in volume of nacre, with the remaining 5% consisting of proteins and polysaccharides which act as "mortar", providing cohesion and energy dissipation to the material (Jackson et al., 1988) (Fig. 1a). Nacre is almost as stiff as the mineral it is made of, yet its staggered structure makes it three orders of magnitude tougher (in energy terms) (Espinosa et al., 2009). The controlled "sliding" of the tablets on one another and the associated energy dissipation have been identified as the main source of toughness for nacre (Espinosa et al., 2009; Jackson et al., 1988; Wang et al., 2001) (Fig. 1b). In this type of process zone mechanism, the toughness (as in energy dissipated per increment of crack advance) is largely governed by the energy dissipated per unit volume of material in tension (Barthelat and Rabiei, 2011). This structure and mechanism are so efficient that at least four distinct classes of mollusk shells have independently evolved a staggered microstructure, in a remarkable example of convergent evolution (Vendrasco et al., 2011). Moreover the staggered microstructure is also found in bone (Gupta et al., 2005), tooth enamel (He and Swain, 2008), spider silk (Keten et al. 2010; Gosline et al., 1999) and wood (Fernandes et al., 2011). The recurrence of the staggered arrangement in nature therefore makes it a "Universal" pattern (Espinosa et al., 2009). Genetic algorithm and brute force exploration indeed recently demonstrated that the staggered structure is the most efficient configuration to generate stiffness, strength and toughness simultaneously (Guo and Gao, 2006; Gao, 2006; Barthelat and Mirkhalaf, 2013). Mimicking the staggered structure in synthetic composite has therefore a tremendous potential, which is just starting to be realized in synthetic materials (Espinosa et al., 2009; Dimas et al., 2013; Barthelat and Zhu, 2011; Bonderer et al., 2008; Wegst et al., 2010; Luz and Mano, 2009).

A variety of theoretical and numerical models have been developed in the past to aid the understanding of natural staggered materials and to establish design guidelines for bio-inspired synthetic composites. Relatively simple two-dimensional theoretical models are available to predict basic properties such as stiffness (Jager and Fratzl, 2000; Kotha et al., 2001; Bar-On and Wagner, 2013), strength (Jackson et al., 1988; Gao, 2006) and toughness (Espinosa et al., 2009; Gao, 2006; Okumura and de Gennes, 2001; Shao et al., 2012). More sophisticated numerical models captured the details of deformation and crack propagation mechanisms in two and three-dimensional structures (Dimas et al., 2013; Barthelat et al., 2007; Katti et al., 2001). The insights emerging from these models are very useful to the designer of nacre-like materials. For example, the size of the inclusions should be small to increase their strength (Currey, 1977; Gao et al., 2003). The overlap between the tablets should be large to promote high stiffness, strength and toughness, but the overlap should be within limit imposed by the fracture of the tablets themselves (Jackson et al., 1988; Gao, 2006; Bonderer et al., 2008; Barthelat et al., 2013). Optimum overlaps associated to the length of the cohesive zone within the interface (Chen et al., 2009) or to optimum strain energy storage (Wei et al., 2012) were also proposed. In addition recent contributions have attempted to develop unified guidelines for the design and fabrication of nacre-like materials (Bonderer et al., 2008; Wei et al., 2012). In particular Begley et al. (2012) have recently proposed systematic design guidelines and comparisons with synthetic nacre-like materials. They established deformation maps for staggered composites, suggested materials for the inclusions and their interface, and provided guidelines for the size of the inclusions. Gao, (2006) examined how the staggered structure addresses the problems of high stiffness, high strength and high toughness simultaneously, and also examined the effect of structural hierarchy on overall performance . This idea was explored in more details by Zhang et al. (2011), who concluded that there are specific numbers of hierarchical levels which maximize overall toughness (strength decreases continuously as additional levels of structural hierarchy are added).

Despite progress in integrating models into unifying design guidelines, there are still limitations and drawbacks to the proposed approaches. For example it is recognized that increasing the aspect ratio of the inclusions can lead to higher performance, with limitations dictated by the strength of the inclusions themselves (Jackson et al., 1988; Gao, 2006; Bonderer et al., 2008; Barthelat et al., 2013). The failure of the inclusions is typically modeled with a criterion based on

maximum average stress across the inclusions, but this criterion was recently shown to overestimate their overall strength (Barthelat et al., 2013). In addition, recommendations from different models are contradictory. For example high mineral content promotes stiffness and strength, but is detrimental to energy absorption and toughness. While it is known that many of the design parameters have contradicting effects on strength and toughness (Barthelat and Rabiei, 2011; Gao, 2006; Begley et al., 2012; Zhang et al., 2011), a multi-objective optimization of stiffness, strength and toughness has not so far been attempted. As a result, there is currently no systematic approach to resolve the conflicting effects of some of the structural design parameters. Finally, other sets of design parameters have similar effects on basic properties. For example increasing tablet overlap and increasing the strength of the interfaces have similar effect on overall strength, so that an infinite number of their combinations may lead, in theory, to the same properties. Whether there is a particular combination of interface strength and tablet overlap which maximizes performance is currently unknown. While previous guidelines suggest specific materials for the inclusions and their interfaces (Begley et al., 2012), material selection was never formally integrated into the optimization process. Despite these various models and guidelines, the designer is therefore still left to struggle with material choice and optimum structure, and the design of optimum synthetic staggered composites is still largely based on trial and error.

In this paper we propose a systematic approach to incorporating the existing models into unified guidelines formulated with the needs of the designer in mind. Existing models for modulus, strength and energy absorption are integrated into a multi-objective optimization scheme which integrates not only microstructural design, but also the material properties of the inclusions and of their interfaces as design parameters. The results lead to step-by-step guidelines to choosing materials for the interfaces and tablets, tablet aspect ratio, volume concentration of tablets and length scale, all for any desired combination of optimum stiffness, strength and toughness. The results of this new design procedure are compared to the structure of natural nacre, and the implications for the design of modern bio-inspired composites are discussed.

2. Representative volume element (RVE): overview

In general, staggered composites are composed of inclusions with a high aspect ratio, and aligned with the direction of loading (Fig. 2). Here we focus on a nacre-like material for which the inclusions are tablets. The tablets may have a relatively well-defined arrangement with a narrow range of overlap length (columnar, Fig. 2a) or a more random arrangement where the position of the tablet across layers shows no correlation (sheet, Fig. 2b). The mechanics of any of these two configurations may be captured by a representative element (RVE) whose behavior is assumed to represent the entire material. The staggered microstructure is three dimensional, which can be computationally expensive to capture in models. Therefore a two-dimensional RVE (Fig. 2c) is typically used to predict modulus, strength, energy absorption and strain at failure for the composite material. Staggered microstructures are found in natural materials and tissues whose primary function is to withstand uniaxial or biaxial tension, and the inclusions (rods, fibers or tablets) are always aligned with the direction of tensile load. For example, strands of spider silk function as ropes which must carry tensile forces. The beta sheet crystals are aligned with the strand, in order to maximize mechanical performance when the strand in loaded in tension (Gosline et al., 1999). The function of mollusk shells is to protect the soft tissues of the animal against predator's bites or debris and rocks displaced by underwater currents and waves. The localized forces generated by these threats generate bending stresses in the shell, where the nacreous layer is in biaxial tension within a plane tangential to the inner surface of the shell (Yourdkhani et al., 2011). The microstructure of nacre maximizes performance for this loading mode, with tablets aligned with the direction of in-plane tensile stresses. Although other loading modes (transverse shear, compression) may also exist for biological or bio-inspired composites, the primary function of staggered composites is to generate stiffness, strength and toughness along the direction of the inclusions. For this reason, most of the models developed in the past for

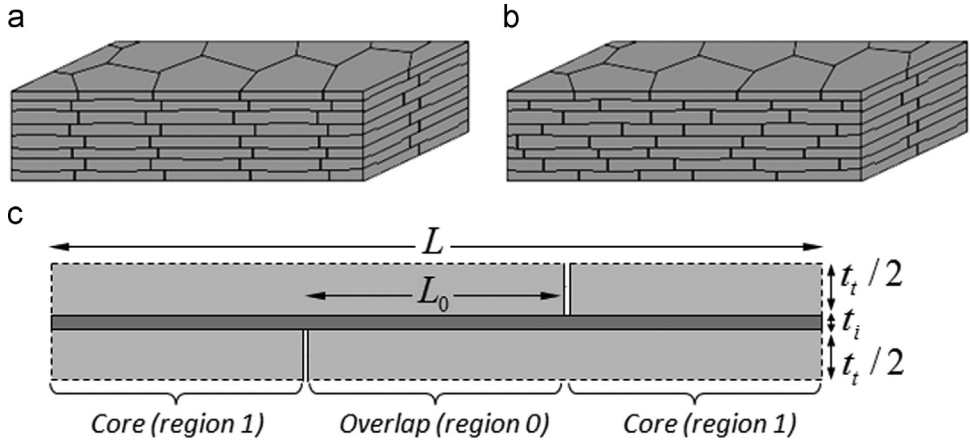

Fig. 2. Two possible arrangements for the tablets (a) columnar and (b) sheet (random); (c) the mechanical response of these different arrangements can be captured with a representative volume element (RVE) subjected to periodic boundary conditions.

staggered composites focus on uniaxial tension along the direction of the tablets. In this work we therefore also focus on tensile loading along the direction of the tablets. The model is subjected to periodic boundary conditions along and across the directions of the tablets. The conditions are enforced by imposing periodicity on the displacements or on the tractions (Kotha et al., 2001; Wei et al., 2012), which is equivalent since the microstructure is periodic (Barthelat et al., 2007). This two-dimensional approach is only an approximation, which is nevertheless useful to draw trends in terms of prediction of properties and design guidelines. The key microstructural parameters are the tablet length L, the overlap length L_0, the tablet thickness t_t and the interface thickness t_i. In some models presented in the past the tablets automatically fully overlap, i.e. $L_0 = \frac{1}{2}L$. The overlap in natural and engineered materials can be much smaller, which has significant impacts on mechanical properties. Therefore in this work we consider the full range of overlap: $0 < L_0/L \leq 0.5$. Actual biological and engineering structures display spatial variations in overlap lengths, following distributions which can be relatively narrow (as in the case of columnar nacre and some synthetic micro-composites) or very wide and even uniform (as in the case of sheet nacre and synthetic nano-composites). It is generally accepted that modeling these complex micro-structures with a single unit cell gives a reasonable representation of the mechanical response of the material, which is sufficiently reliable to examine trends and establish broad design guidelines.

Using the dimensions of the structure the volume fraction of the tablets can be written

$$\phi = \frac{t_t}{t_t + t_i} \tag{1}$$

It is also useful to define the aspect ratio for the tablets

$$\rho = \frac{L}{t_t} \tag{2}$$

And the aspect ratio of the overlap region

$$\rho_0 = \frac{L_0}{t_t} \tag{3}$$

Finally the overlap ratio κ can be written

$$\kappa = \frac{L_0}{L} = \frac{\rho_0}{\rho} \text{ with } 0 < \kappa \leq 0.5 \tag{4}$$

For the case of fully overlapping tablets, $\kappa = 0.5$(symmetric RVE (Begley et al., 2012)). If the arrangement of the tablets does not show any spatial relationship across layers, then the overlap length of the tablets obeys a uniform probability distributed over $0 < \kappa \leq 0.5$, leading to an average overlap ratio of $\kappa = 0.25$.

3. Properties of the tablets and interfaces

The tablets are made of a linear elastic and brittle material with modulus E_t and fracture toughness K_{IC}. The objective of the models is to draw global trends and guidelines, for which only approximations for the materials parameters are sufficient. The effects of the Poisson's ratio for the tablets are therefore neglected to simplify the calculations. The tensile strength of the brittle tablets is governed by linear fracture mechanics, and it is given by

$$\sigma_t = \frac{K_{IC}}{f_0\sqrt{\pi a}} \tag{5}$$

Where a is the length of an edge defect in the tablet and f_0 is a non-dimensional geometrical factor given by (Tada et al., 2000)

$$f_0(a/t_t) = 1.12 - 0.23(a/t_t) + 10.6(a/t_t)^2 - 21.8(a/t_t)^3 + 30.4(a/t_t)^4 \tag{6}$$

The only energy that the tablets absorb upon failure is by generating new surfaces, which is extremely small compared to the amount of energy dissipated at the visco-plastic interfaces. We therefore neglect the amount of mechanical energy absorbed by the tablets ($U_t \approx 0$). The interfaces are modeled as linear elastic-perfectly plastic with modulus E_i, strength σ_i and tensile strain at failure ε_i. Assuming that the yielding of the interfaces is governed by Von Mises plasticity, the shear strength of the interface is given by

$$\tau_i = \frac{\sigma_i}{\sqrt{3}} \tag{7}$$

The shear strain at failure of the interface is given by Shrivastava et al. (1982):

$$\gamma_i = \sqrt{3}\varepsilon_i \tag{8}$$

Neglecting the amount of elastic energy stored and released in the interface, the energy dissipated per unit volume of interface material is therefore

$$U_i = \sigma_i\varepsilon_i = \tau_i\gamma_i \tag{9}$$

The following sections will now examine the mechanical response of the RVE as function of the microstructural parameters and materials properties for the tablet (E_t, K_{IC}) and the interfaces ($E_i, \sigma_i, \varepsilon_i$).

4. Basic mechanical properties

In the models presented below we assume that the ends of the tablets are free i.e., there is no material between the vertical junctions in the tablets. The solutions used below are therefore simplified and focus on capture the main mechanism associated with the RVE, which is a "shear–tension–shear" configuration (Jager and Fratzl, 2000; Kotha et al., 2001) where the tablets are in tension and the interfaces are in shear. Material at the vertical junctions stiffen and strengthen the composite (Begley et al., 2012; Bekah et al., 2011; Bar-On and Wagner, 2011). These junctions fail in tension either by adhesive or cohesive failure, but their contribution on post yield behavior is difficult to assess since tough synthetic and biological composites tend to form ligaments in tension (Jackson et al., 1988; Smith et al., 1999). The tensile stress in the tablets and the shear stress in the interface are, in general, not uniform. The exact profile of these stresses in the elastic and elastic–plastic regimes are important to determine the quality of the load transfer between tablets, properties such as composite modulus, and to predict the fracture of the tablets. Focusing on an individual overlap region within the composite, the distribution of shear stresses along the interface is governed by a nondimensional "elastic shear transfer" number (Kotha et al., 2001; Wei et al., 2012; Volkersen, 1938) which can be written (Barthelat et al., 2013)

$$\beta_0 = \rho_0 \sqrt{\frac{G_i}{E_t}\frac{t_t}{t_i}} \tag{10}$$

Here ρ_0 is the overlap ratio, G_i is the shear modulus of the interfaces, E_t is Young's modulus of the tablets, and t_t and t_i are the thicknesses of the tablets and interfaces, respectively. Using Eq. (1) and assuming $G_i = E_i/3$ for an incompressible interface, Eq. (10) can be written

$$\beta_0 = \rho_0 \sqrt{\frac{1}{3}\frac{E_i}{E_t}\frac{\phi}{1-\phi}} \tag{11}$$

Where ϕ is the volume concentration of the tablets. For $\beta_0 \approx 1$ or smaller, the shear stress is quasi-uniform along the overlap length. This case corresponds to staggered composites where the interfaces are significantly softer than the tablets (i.e. lower interface modulus and/or high interface thickness), and/or small overlap ratio ρ_0. On the other hand, for larger β_0 the shear stresses become more concentrated near the ends of the overlap regions, For larger values of β_0 the shear stress completely vanishes over a characteristic distance $L_0/2\beta_0$ from the ends of the overlap region (Chen et al., 2009). In all cases the shear stress decreases abruptly to zero at the free surface (Adams and Peppiatt, 1974). In addition to high shear stresses, peel stresses (tensile stress perpendicular to the interfaces) also appear at the ends of the overlap regions for high values of β_0 (Barthelat et al., 2013). In this case the ends of the interfaces can be regarded as stress concentrations which accelerate failure and are therefore detrimental. Large values of β_0 also lead to less efficient structures: for $\beta_0 \approx 10$ and higher, the interface located in the central region of the overlap region does not carry any stress, and does not provide any contribution to the structural performance of the composite. Finally, inhomogeneous shear stress transfer increases the risk of fracturing the tablets as discussed in Section 5 of this article. For the extreme case where $\beta_0 = +\infty$, shear stresses are transferred through pairs of point forces applied at the ends of the overlap regions (Barthelat et al., 2013). This extreme case can serve as the basis for the conservative form of the design guidelines.

4.1. Modulus

Using the profile of shear stress at the interfaces as well as the tensile stress field within the tablets Kotha et al. (2001) computed the modulus of the composite RVE in tension along the direction of the tablets, assuming that the interface do not carry tensile stresses. Their result can be written in the simplified form

$$E = \frac{\phi E_t}{1 + \coth(\beta_0)/\beta_0} \tag{12}$$

Where ϕ is the tablet concentration, E_t is the tablet modulus, and β_0 is the shear transfer parameter given by Eq. (11). This model is based on a simple form of the shear–tension model where there are no gaps and no matrix at the ends of the tablets. Adding matrix material at the ends of the tablets provides additional stiffness and strength (Bekah et al., 2011), and the effect of gaps can also be significant (Bar-On and Wagner, 2013). In addition, confinement effects at the ends of the tablets can generate additional stiffness which can be appreciable when the interface approach the incompressibility limit (Liu et al., 2006). These more complex cases were not considered here for the sake of simplicity. We however used an improved version of the shear–tension model by considering the case of a non-symmetric RVE (Begley et al., 2012; Yourdkhani et al., 2011) made of an overlap region of length $L_0 = \kappa L$, and of a core region of length $L - L_0 = (1-\kappa)L$ When this asymmetric RVE is subjected to tension the two regions act in series, so that the modulus of the composite is given by

$$\frac{1}{E_c} = \frac{\kappa}{E_0} + \frac{1-\kappa}{E_1} \tag{13}$$

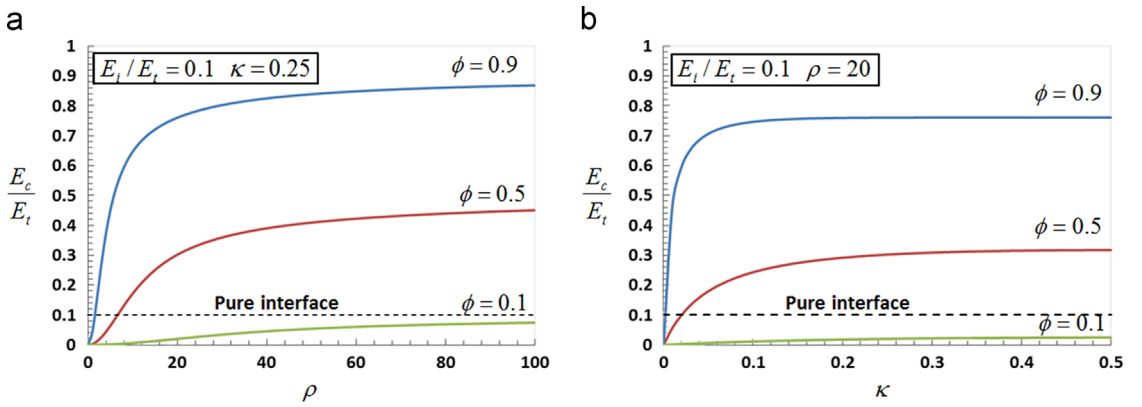

Fig. 3. (a) Normalized stiffness as function of tablet aspect ratio ρ for three different tablet concentrations and for $E_i/E_t = 0.1$ and $\kappa = 0.25$. All concentrations converge towards the Voigt composite model for large aspect ratios. (b) normalized stiffness as function of overlap ratio κ for three different tablet concentrations and for $E_i/E_t = 0.1$ and $\rho = 20$.

Where E_0 is the tensile modulus of the overlap region of the RVE and E_1 is the tensile modulus of the core region of the RVE. Using Eq. (12) but replacing β_0 with $\beta_1 = \frac{1-\kappa}{\kappa}\beta_0$ for the core region leads to

$$E_c = \frac{\phi E_t}{1+\frac{\kappa}{\beta_0}\left[\coth(\beta_0) + \coth\left(\frac{1-\kappa}{\kappa}\beta_0\right)\right]} \text{ with } \beta_0 = \kappa\rho\sqrt{\frac{1}{3}\frac{E_i}{E_t}\frac{\phi}{1-\phi}} \tag{14}$$

This result is similar to the studies on non-symmetric RVEs by Yourdkhani et al. (2011) and Begley et al. (2012). The solution presented here is however simpler because the vertical junctions were not included. Eq. (14) shows that the modulus is simply function of the tablet modulus E_t, tablet concentration ϕ, load transfer number β_0 and overlap ratio κ. Fig. 3a shows how the modulus initially rapidly increases with aspect ratio, and converges towards $\lim_{\rho\to+\infty}(E_c) = \phi E_t$ which is simply the Voigt composite model for the case where the interfaces do not carry any tensile stress (note that the Reuss lower bond is zero since the RVE contains crack-like initial features with zero modulus). Higher tablet concentrations lead to higher composite modulus, and also make the modulus converge towards the Voigt limit faster. Fig. 3b shows how the modulus increases with the overlap ratio κ, with the maximum modulus occurring when the tablets fully overlap, i.e. for $\kappa = 0.5$. The modulus approaches this maximum value faster for higher concentration. For example for $\phi = 0.9$ the modulus reaches 90% of its maximum value ($\kappa = 0.5$) for $\kappa = 0.04$. This result implies that for high tablet concentrations, variations in overlap ratios have little effects on the overall modulus, an interesting results exploited in natural materials. In summary high tablet concentrations not only lead to higher modulus, they also lead to configurations which are less sensitive to aspect ratio and overlap ratio, resulting in more robust microstructures. On the other hand, combinations of low values for ρ, κ and ϕ lead to very low values for the modulus, in some cases even below the modulus of the interfaces themselves (dashed lines on Fig. 3a and b). In particular, if ϕ is too low (ϕ=0.1 is shown on Fig. 3), the modulus of the composite is below the modulus of the interface. For these cases the staggered structure is therefore detrimental to stiffness. Changing the contrast of stiffness E_i/E_t between interface and tablet changed the absolute values for the composite stiffness, but not the overall trends and general observations.

4.2. Strength and optimal load transfer

For the case of ductile interfaces and if $\beta_0 > 0$, yielding will initiate first at the ends of the overlap region from the combined effect of high shear stresses and peel stresses at these locations. As the tensile stress on the RVE is increased the plastic region will propagate towards the middle of the overlap (Kotha et al., 2001; Wei et al., 2012). Once the interface is fully yielded and if the interface is perfectly plastic the shear stresses are uniform and the peel stresses vanish, a configuration which becomes similar to the elastic case $\beta_0 = 0$ discussed above. For simplicity we take the point where the interface has fully yielded as the yield point for the RVE and for the staggered composite. Upon yielding of the interface the maximum force carried by the tablet is $L_0\tau_i$, and neglecting the tensile stress carried by the interface the strength of the RVE is

$$\sigma_c = \frac{L_0\tau_i}{t_t + t_i} \tag{15}$$

Which can be rewritten using Eqs. (1) and (3)

$$\sigma_c = \phi\rho_0\tau_i \tag{16}$$

This equation is similar to the results presented in Gao (2006), Bekah et al. (2011) Begley et al. (2012). The present result is however more general because it includes asymmetric cases where $\kappa < 0.5$. Eq. (16) shows how the strength of the

interfaces is amplified by the factor $\phi\rho_0$ in the staggered composite. It also suggests that the staggered structure does not guarantee a composite strength higher than the strength of the interface material. The tablets strengthen the material only if $\sigma_c > \sigma_i$ or if

$$\phi\rho_0 > \sqrt{3} \tag{17}$$

The implication is similar to modulus: in terms of strength, the staggered structure is only advantageous for high tablet concentration and/or high overlap between tablets. Eq. (16) also assumes that the interface fully yields before the shear strain at the ends of the overlap region reaches its maximum value γ_i. This condition was examined by Gao (2006), Chen et al. (2009), who considered the length λ of the cohesive zone:

$$\lambda = t_t\sqrt{\frac{E_t}{\tau_i}\frac{1-\phi}{\phi}\gamma_i} \tag{18}$$

Where τ_i is the shear strength of the interface and γ_i is the shear strain at failure. The condition for the entire overlap region to yield before the interface entirely fails at the ends of the overlap region is $L_0 \le 2\lambda$, or

$$\rho_0 \le 2\sqrt{\frac{E_t\gamma_i}{\tau_i}\frac{1-\phi}{\phi}} \tag{19}$$

Eq. (19) can be interpreted as a condition for the interface to fail in a ductile fashion, as opposed to a brittle failure. Importantly, this result implies that even with a relatively "ductile" material at the interface, the composite may fail in a brittle fashion if the overlap length is too large.

4.3. Strain at failure

If the overlap region is smaller than the core region and if no hardening mechanism operates at the interface (as assumed above), yielding will only occur in the overlap region by way of the "weakest link" principle. The strain produced by the core region therefore becomes negligible in the post-yield regime, and the tensile strain at failure for the composite is simply given by

$$\varepsilon_c = \frac{1-\phi}{\phi}\frac{1}{\rho}\gamma_i \tag{20}$$

Where γ_i is the shear strain at failure of the interface. The strain at failure ε_c is larger for lower tablet concentration and smaller overlap ratio, which highlights contradictory effects in this material: while high tablet concentrations and high overlap ratios lead to high modulus and strength, they result in smaller strains at failure and in materials which are more brittle. In terms of strain at failure the staggered structure is also only advantageous only if the strain at failure of the composite is greater than the strain at failure of the brittle tablets. This condition can be written:

$$\frac{1-\phi}{\phi}\frac{1}{\rho}\gamma_i > \varepsilon_t \tag{21}$$

Where $\varepsilon_t = \sigma_t/E_t$. On the other hand, the strain at failure for the composite may also be greater than the strain at failure of the interface material. The condition for this case is obtained by replacing Eqs. (8) and (20) into $\varepsilon_c > \varepsilon_i$ giving

$$\frac{1-\phi}{\phi}\frac{1}{\rho} > \frac{1}{\sqrt{3}} \tag{22}$$

Eq. (22) shows that the staggered structure may also amplify the strain at failure of the interface material because of the way the tablets channel shear deformations.

4.4. Energy absorption

The energy absorption of the composite is defined as the amount of mechanical energy absorbed per unit volume of the composite when it is deformed up to failure. The energy absorption is an important property which has a direct influence on toughness and on resistance to cracking (Espinosa et al., 2009; Shao et al., 2012). The tablets are assumed to be linear elastic and therefore only the interfaces at the overlap region absorb energy. The energy absorption for the composite is then given by

$$U_c = \sigma_c\varepsilon_c = \kappa\tau_i\gamma_i(1-\phi) \tag{23}$$

The energy absorption decreases linearly as the volume fraction of the tablets increases, since the tablets do not absorb energy. In addition, since only a fraction κ of the interface dissipates energy, larger overlap ratios lead to higher energy dissipation. The basic tensile properties of the RVE are summarized in Table 1. These models are identical or similar to those developed in the past for staggered composites (Gao, 2006; Kotha et al., 2001; Wei et al., 2012; Begley et al., 2012; Bar-On and Wagner, 2013; Lei et al., 2013).

Table 1
Models for the tensile properties of the RVE.

"Elastic shear transfer" number	$\beta_0 = \rho_0 \sqrt{\frac{1}{3}\frac{E_i}{E_t}\frac{\phi}{1-\phi}}$
Composite modulus	$E_c = \frac{\phi E_t}{1+\frac{\kappa}{\beta_0}\left[\coth(\beta_0) + \coth\left(\frac{1-\kappa}{\kappa}\beta_0\right)\right]}$
Composite strength	$\sigma_c = \phi\rho_0\tau_i$
Composite energy absorption	$U_c = \kappa\tau_i\gamma_i(1-\phi)$
Composite strain at failure	$\varepsilon_c = \frac{1-\phi}{\phi}\frac{1}{\rho}\gamma_i$

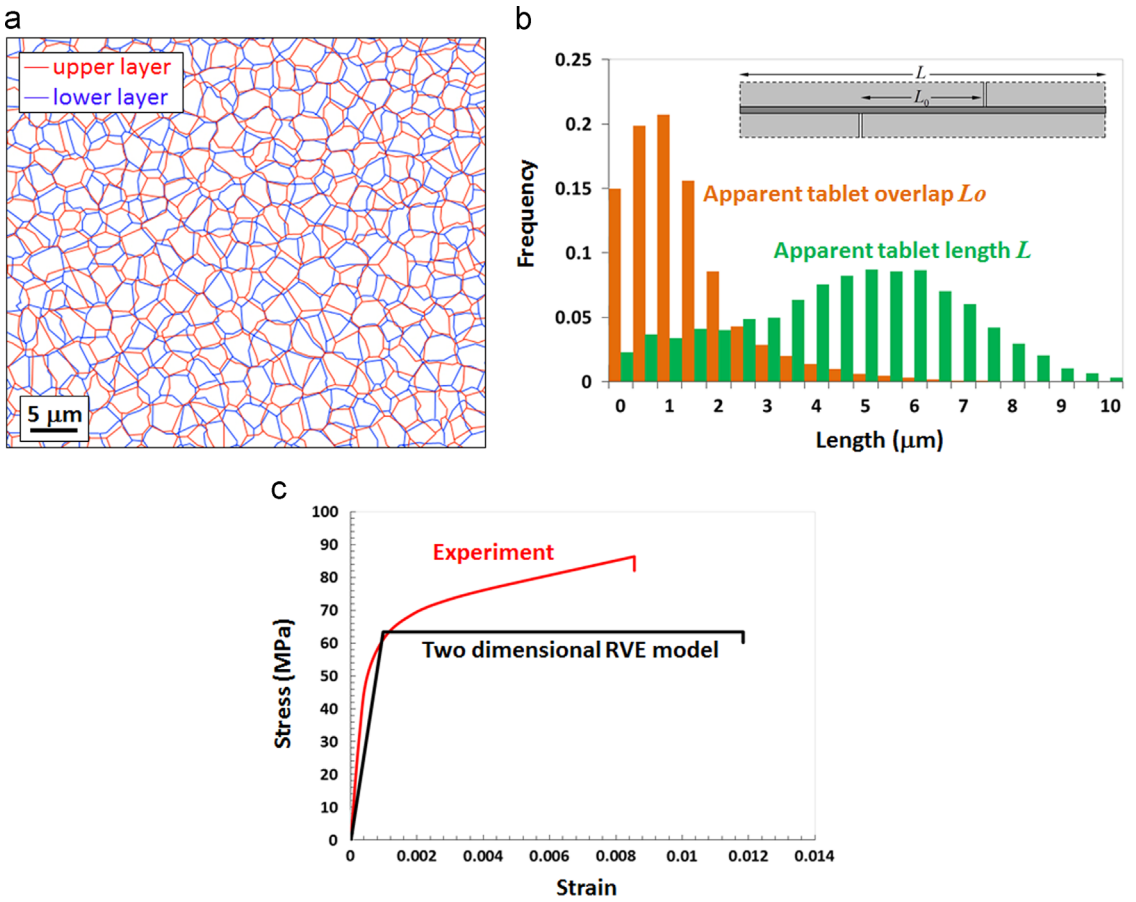

Fig. 4. (a) Contours of the tablets from two consecutive layers in red abalone; (b) distribution of the tablet length and the overlap length obtained from image analysis; (c) experimental (from (Barthelat et al., 2007)) and predicted tensile stress strain curves for red abalone nacre.

4.5. Comparison with nacre

We can now compare these predictions with experimental results for nacre from red abalone. For nacre $\phi \approx 0.95$. The thickness of the tablets in red abalone is $t = 0.45$ μm obtained from cross section images of nacre (Barthelat et al., 2007). The tablet length and overlap is more difficult to obtain, because of the complex three-dimensional architecture of nacre. Reasonable estimate can however be obtained by analysis of the contours of the tablets from two consecutive layers, obtained from optical microscopy (Barthelat et al., 2007) (Fig. 4a). The apparent length of the tablet can be determined by measuring the intersect length between a straight line (line probe) and the two dimensional contours of the tablets. We have used horizontal and vertical line probes on Fig. 4a to obtain the statistics of Fig. 4b. Line probes at any other angles give the same average and standard deviation for the overlap, showing that the structure is isotropic in plane. The results of this analysis (Fig. 4b) give $L \approx 6$ μm and $L_0 \approx 1$ μm (Note that the overlap length can be as large as $2-3$ μm). Together these values give $\rho \approx 13$, and $\kappa \approx 0.17$.

Previous experiments on the mineral tablets in nacre gave $E_t \approx 100$ GPa (Barthelat et al., 2006), and shear tests gave $E_i = 3G_i \approx 2.4$ GPa and $\tau_i \approx 30$ MPa (Barthelat et al., 2007), with hardening up to 50 MPa at a failure strain of $\gamma_i = 3$.

These values give $\beta_0 \approx 1$, indicating that the elastic load transfer at the interface is close to uniform, producing an optimal load transfer at the interface. The full stress strain curve predicted by the equations in Table 1 is shown on Fig. 4c. The RVE model agrees well with the experiments considering it is only a two-dimensional model. The experiment is showing larger stress in the post-yield region because of strain hardening (Barthelat et al., 2007).

4.6. Non-dimensional formulation

Since the equations in Table 1 are not size-dependent they can be more conveniently formulated in non-dimensional forms. To guide this process it is useful to examine the effects of some of these parameters. For example the shear strain at failure of the interface γ_i only affects energy absorption and strain at failure, and should always be maximized to maximize U_c, which also ensures that the condition for optimal shear transfer in the post-yield regime (Eq. (19)) is met. Likewise, the modulus of the tablets E_t should always be maximized to achieve high composite stiffness. High aspect ratio of the tablets increases stiffness and strength, with no impact on energy absorption. The highest possible aspect ratio should be selected, the limit being governed by the fracture of the tablets themselves (this limitation is examined in details in the next section). The strength of the tablets σ_t should therefore always be maximized. These observations suggest a non-dimensional formulation where the properties and parameters are normalized by the properties which should always be maximized (E_t, σ_t and γ_i)

$$\begin{cases} \tilde{\sigma} = \frac{\sigma}{\sigma_t} \\ \tilde{\varepsilon} = \frac{\varepsilon}{\varepsilon_t} \\ \tilde{\gamma} = \frac{\gamma}{\varepsilon_t} \end{cases}, \begin{cases} \tilde{E}_i = \frac{E_i}{E_t} \\ \tilde{\tau}_i = \frac{\tau_i}{\sigma_t} \\ \tilde{U}_i = \frac{U_i}{\sigma_t \gamma_i} = \tilde{\tau}_i \\ \tilde{\gamma}_i = \frac{\gamma_i}{\varepsilon_t} \end{cases}, \begin{cases} \tilde{E}_t = 1 \\ \tilde{\sigma}_t = 1 \\ \tilde{U}_t = 0 \\ \tilde{\varepsilon}_t = 1 \end{cases} \tag{24}$$

Normalizing the modulus and strength by the modulus and strength of the tablets leads to normalizing the strains by the strain at failure for the tablets $\varepsilon_t = \sigma_t / E_t$. A special attention is given to energy absorption, which is normalized by the energy of a hypothetical material which would have the strength of the tablets and the elongation of the interfaces. Choosing this normalization scheme, the three key properties $(\tilde{E}, \tilde{\sigma}, \tilde{U})$ are always between 0 and 1 for the interfaces, the tablets and the composite. For the tablets the energy stored is recoverable and does not dissipate, and therefore $\tilde{U}_t = 0$. The normalized properties for the composite then become

$$\begin{cases} \tilde{E}_c = \frac{E_c}{E_t} = \frac{\phi}{1 + \frac{\kappa}{\beta_0}\left[\coth(\beta_0) + \coth\left(\frac{1-\kappa}{\kappa}\beta_0\right)\right]} \\ \tilde{\sigma}_c = \frac{\sigma_c}{\sigma_t} = \phi \rho_0 \tilde{\tau}_i \\ \tilde{U}_c = \frac{U_c}{\sigma_t \gamma_i} = \kappa \tilde{\tau}_i (1-\phi) \\ \tilde{\varepsilon}_c = \frac{\varepsilon_c}{\varepsilon_t} = \frac{1-\phi}{\phi} \frac{1}{\rho} \tilde{\gamma}_i \end{cases} \quad \text{with } \beta_0 = \kappa\rho \sqrt{\frac{1}{3}\tilde{E}_i \frac{\phi}{1-\phi}} \tag{25}$$

The parameter $\rho_0 = \kappa\rho$ has a special importance for the design of the composite, and should therefore be maximized, within limitations in order to prevent the fracture of the tablets themselves, as presented in the next section.

5. Tablet fracture

In order to preserve the beneficial mechanisms of shear–tension–shear load transfer, tablet sliding (pullout) energy dissipation, and ultimately toughness, the tablets must remain intact. To predict the fracture of the tablets, existing models typically compare the nominal stress carried by the tablets (stress averaged over the cross section) with the tensile strength of the material they are made of. This criterion significantly overestimates the strength of the tablets in the staggered structure, because the staggered structure actually gives rise to stress singularities in the tablets (Bekah et al., 2011). Based on this observation we have recently developed and validated an improved failure criterion for the tablets, using closed-form solutions for stress-intensity factors in elastic strips subjected to point forces (Barthelat et al., 2013). In this model we assumed that the tablets are brittle, and that their failure is governed by linear elastic fracture mechanics. Two versions of the criterion were proposed: a version for cases where the shear transfer is uniform and "optimum" (uniform shear traction, $\beta = 0$) and another version, more conservative, which is based on the extreme case where the shear stress is transferred by point forces at the ends of the overlap regions ($\beta = +\infty$). The two versions of the criteria are illustrated on Fig. 5a and b. The criteria incorporates the toughness of the tablets K_{IC}, their thickness t_t, the relative size a/t_t of the surface defects they initially contain, as well as the shear strength of the interfaces τ_i. Once these parameters are known, the maximum overlap ratio which will prevent the fracture of the tablets can be determined as function of the non-dimensional number $(K_{IC}/\tau_i\sqrt{\pi t_t})$ and the relative defect size in the tablet a/t_t. Fig. 5 shows that for both criteria, larger overlap ratio can be achieved for higher toughness, lower interface strength and smaller tablet size t_t. Smaller relative defect size a/t_t also enable larger overlap ratio, except for $a/t_t < 0.15$, where the crack tip, close to the surface, interacts strongly with the point forces applied at the mouth of the defect. These criteria were validated against actual composites made of alumina tablets and

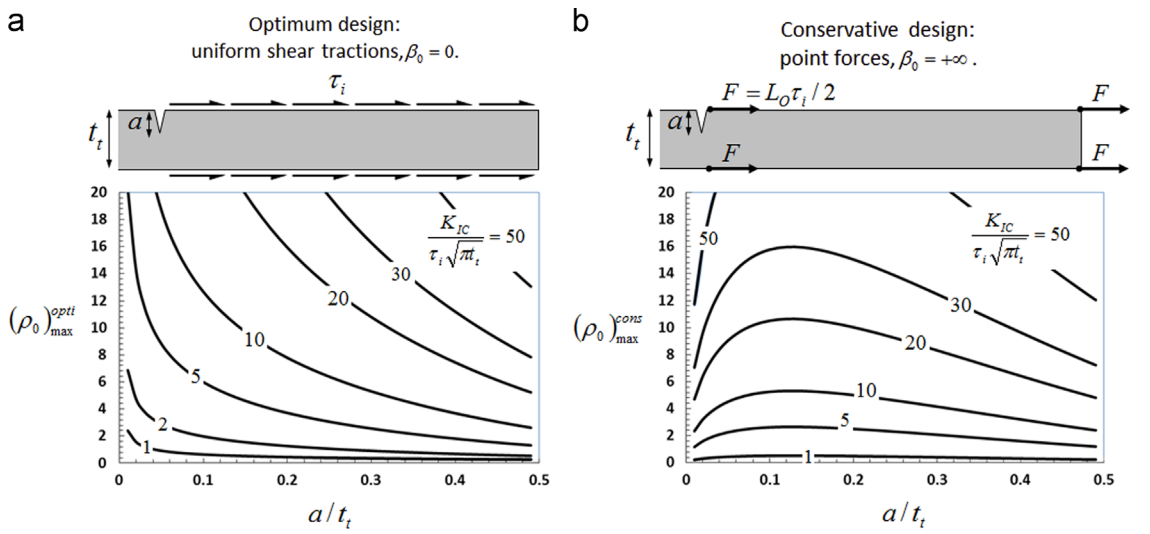

Fig. 5. Diagrams illustrating the failure criteria for the tablets: (a) optimum version based on uniform shear transfer at the interfaces and (b) conservative version based on point force shear transfer at the interfaces.

synthetic polymers at the interfaces (epoxy and polyurethane), and compared well with experimental data on natural nacres.

Here we present a simple form of the criteria which we will use for the design optimization. These criteria can be fitted with relatively simple functions which we present here for the first time. The "optimum" and "conservative" criteria can be fitted with

$$\begin{cases} (\rho_0)^{opti}_{\max} = \frac{1}{2f_0}\frac{K_{IC}}{\tau_i\sqrt{\pi a}} - 2.364\left[\left(\frac{a}{t_t}\right)^{-0.15} - 1.12\right] \\ (\rho_0)^{cons}_{\max} = \frac{1}{2f_0}\frac{K_{IC}}{\tau_i\sqrt{\pi a}}\frac{1}{0.1831\left[\left(\frac{a}{t_t}\right)^{-1} + 3.87\right]} \end{cases} \tag{26a, b}$$

With f_0 defined by Eq. (6). These criteria can also be written in non-dimensional forms

$$\begin{cases} (\rho_0)^{opti}_{\max} = \frac{1}{2\tilde{\tau}_i} - 2.364\left[\left(\frac{a}{t_t}\right)^{-0.15} - 1.12\right] \\ (\rho_0)^{cons}_{\max} = \frac{1}{2\tilde{\tau}_i}\frac{1}{0.1831\left[\left(\frac{a}{t_t}\right)^{-1} + 3.87\right]} \end{cases} \tag{27a, b}$$

The expression $(\rho_0)_{\max} = (1/2\tilde{\tau}_i)$ is the criterion which is traditionally used to predict tablet fracture, and which assumes uniform tension in the tablets. The new "optimum" criterion deviates only slightly from the traditional criterion for large initial defects, but for small defects and for overlap ratios in the range of 1–10, the difference is significant. In the case of the conservative design, the maximum aspect ratio is only 1/5 of the value predicted by the traditional criterion. These differences are significant, indicating the need to incorporate these more sophisticated design criteria for the design of optimum staggered composites. In addition, while the optimum and conservative criteria give similar results for large relative defects, their prediction differ significantly for smaller relative defects. The optimum criterion should only be used in the case where the interface is perfectly plastic with no hardening. If the behavior deviates too much from perfect plasticity, the conservative form should be used. We can now compare the predictions for optimum aspects ratios with the actual microstructure of nacre from red abalone. We take the size of the surface defect equal to $a \approx 50$ nm, which is the size of the nanograins the tablets are made of (Rousseau et al., 2005), and the thickness of the tablets is $t_t \approx 500$ nm. These values give $a/t_t \approx 0.1$. The toughness of the tablets in nacre is not known, but an estimate can be used from the toughness of calcite: $K_{IC} \approx 0.4$ MPa.m$^{1/2}$ (Broz et al., 2006). Using Eq. (5) the tensile strength of the tablets in uniaxial tension is $\sigma_t \approx 900$ MPa. With the ultimate shear strength of the interface $\tau_i \approx 50$ MPa (Barthelat et al., 2007) one obtains $\tilde{\tau}_i \approx 0.055$. Using Eq. (27) these values give the maximum overlap ratio according to the conservative criterion: $(\rho_0)^{opti}_{\max} \approx 8$ and $(\rho_0)^{cons}_{\max} \approx 3.5$. The actual overlap ratio in nacre is overlap ratio is $\rho_0 \approx 1-6$ (Fig. 4b), which is remarkably close to the maximum overlap ratios predicted by these criteria.

6. Optimum designs: achieving stiffness, strength and energy absorption simultaneously

We now explore pathways to optimize the staggered structure for simultaneous stiffness, strength and energy absorption within the limitations given by the failure of the tablets (Eq. (27)). The main objectives are to resolve the contradictory effects of some of the parameters, and to identify optimum microstructures and materials for specific combinations of stiffness, strength and energy absorption. Some of the parameters are easier to optimize, because they have similar effects on all properties. For example higher overlap ratios ρ_0 are desired, with the limit set by tablet fracture. We will therefore use the upper value of the overlap ratio based on the failure criterion of the tablet, focusing on the optimum failure creation: $\rho_0 = (\rho_0)^{opti}_{\max}$ provides an equation which couples ρ_0 and $\tilde{\tau}_i$through Eq. (27a). In the rest of this article we set $\kappa = 0.25$, which corresponds to the case where the tablets follow a uniform statistical distribution over $0 < \kappa < 0.5$. This case is probably the most relevant for many actual synthetic nacre-like materials where the overlap length is random. Interestingly, studies on large scale RVEs which included statistics over hundreds of tablets suggested that the mechanical response is largely governed by the average value for the main structural parameters, and that the width of the statistical distribution plays a much lesser role (Rabiei et al., 2010; Rabiei et al., 2012). Here we also assume that $\tilde{\gamma}_i$ satisfies Eq. (19), that is $\tilde{\gamma}_i$ is sufficiently large to ensure optimum shear transfer in the post yield regime. As discussed in the design guidelines below, the optimum composites will use interfaces which are deformable enough to satisfy this requirement. $\tilde{E}_i$ contributes to composite modulus only, and should always be maximized. In the context of selecting a candidate material of the interface, we note that materials which are stiff are also typically strong (Ashby, 1999). Using this general trend and to streamline our choice of materials, we assume that $(E_i/E_t) \approx (\tau_i/\sigma_t)$, or in non-dimensional form: $\tilde{E}_i \approx \tilde{\tau}_i$. This approximation will enable us to establish coarse design guidelines on the choice of the materials, which can be refined once the materials are chosen. The optimization problem therefore reduces to identifying optimum values for $\tilde{\tau}_i$ and ϕ. Fig. 6 shows the effect of these two parameters on modulus, strength and energy absorption, and highlights some of their contradictory effects: larger tablet

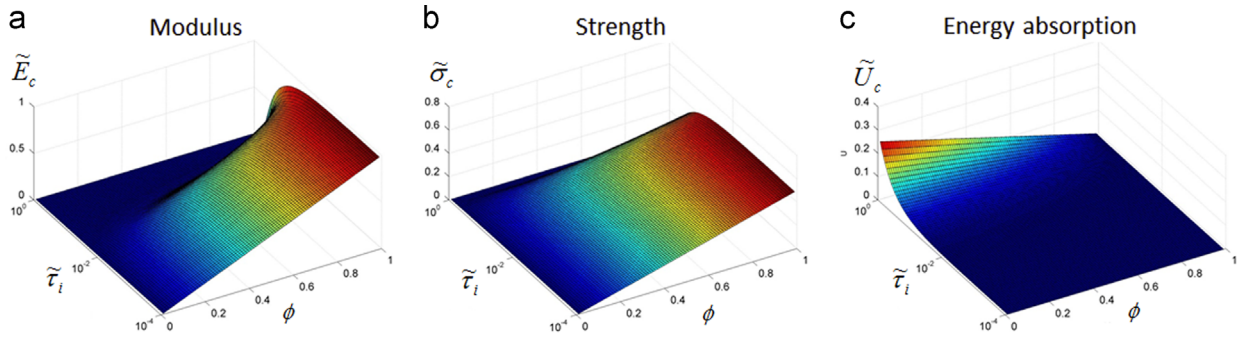

Fig. 6. Properties of the composite as function of relative interface strength and tablet volume concentration: (a) modulus, (b) strength and (c) energy absorption as function of relative interface strength and tablet concentration. For all plots $a/t_t = 0.1$.

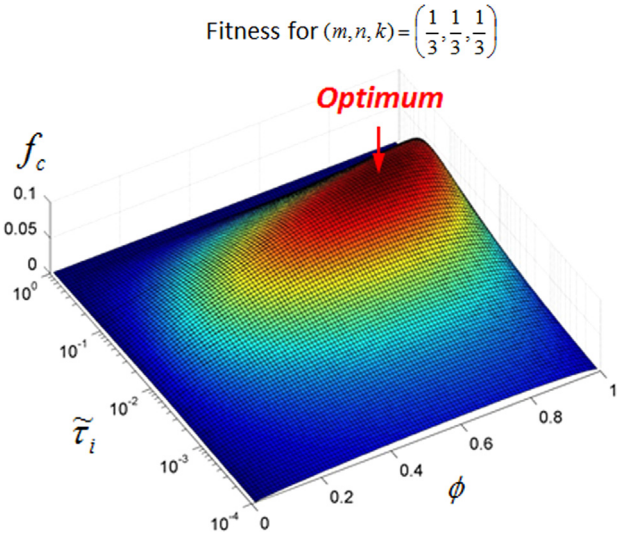

Fig. 7. Composite fitness as function of relative interface strength and tablet concentration. Here $a/t_t = 0.1$ and $(m,n,k) = (1/3, 1/3, 1/3)$. The optimum failure criterion was used.

concentrations ϕ increase modulus and strength, but decrease energy absorption. Smaller $\tilde{\tau}_i$ increase modulus because they enable higher overlap length between the tablets, but smaller $\tilde{\tau}_i$ also reduce energy absorption.

In order to resolve these contradictions, we use a multi-objective optimization approach. In this case we use a weighted product approach (Marler and Arora, 2004) where the multi-objective function, or "fitness" is written

$$f_c = \tilde{E}_c^m \tilde{\sigma}_c^n \tilde{U}_c^k \tag{28}$$

$\tilde{E}_c, \tilde{\sigma}_c, \tilde{U}_c$ are the non-dimensional properties of the composite and m, n, k are non-dimensional indices for which we require $m+n+k=1$. These indices can be modulated to change the emphasis on particular properties. For example $(m,n,k)=(0.45, 0.45, 0.1)$ produces a fitness function which puts more emphasis on stiffness and strength, and less on energy absorption. The particular multi-objective function pf Eq. (28) was chosen because (i) it is mathematically simple; (ii) it gives a balanced weight to each property, even though they are numerically different by orders of magnitude and (iii) the weight of each of the properties can be easily tuned while maintaining $m+n+k=1$, making the ternary diagram representation possible. Once the indices m, n, k are chosen, f_c can be maximized through the two independent design parameters $\tilde{\tau}_i$ and. Fig. 7 shows how this approach can resolve the conflicting effects of ϕ and $\tilde{\tau}_i$. In this example $m=n=k=1/3$, and the fitness function has a maximum value of about 0.1 for an optimum combination of $\phi \approx 0.75$ and $\tilde{\tau}_i \approx 0.1$.

More generally, the optimum values of ϕ and $\tilde{\tau}_i$ depend on the chosen combination of (m, n, k), and this choice ultimately depends on the function of the material. Therefore to stay in the general case we now consider the optimum values of the design parameters as function of any combination of (m, n, k). Since $m+n+k=1$, the optimum microstructures can be displayed in a ternary diagram (Fig. 8), in which all possible combinations of (m, n, k) occupy a triangular space. The lower

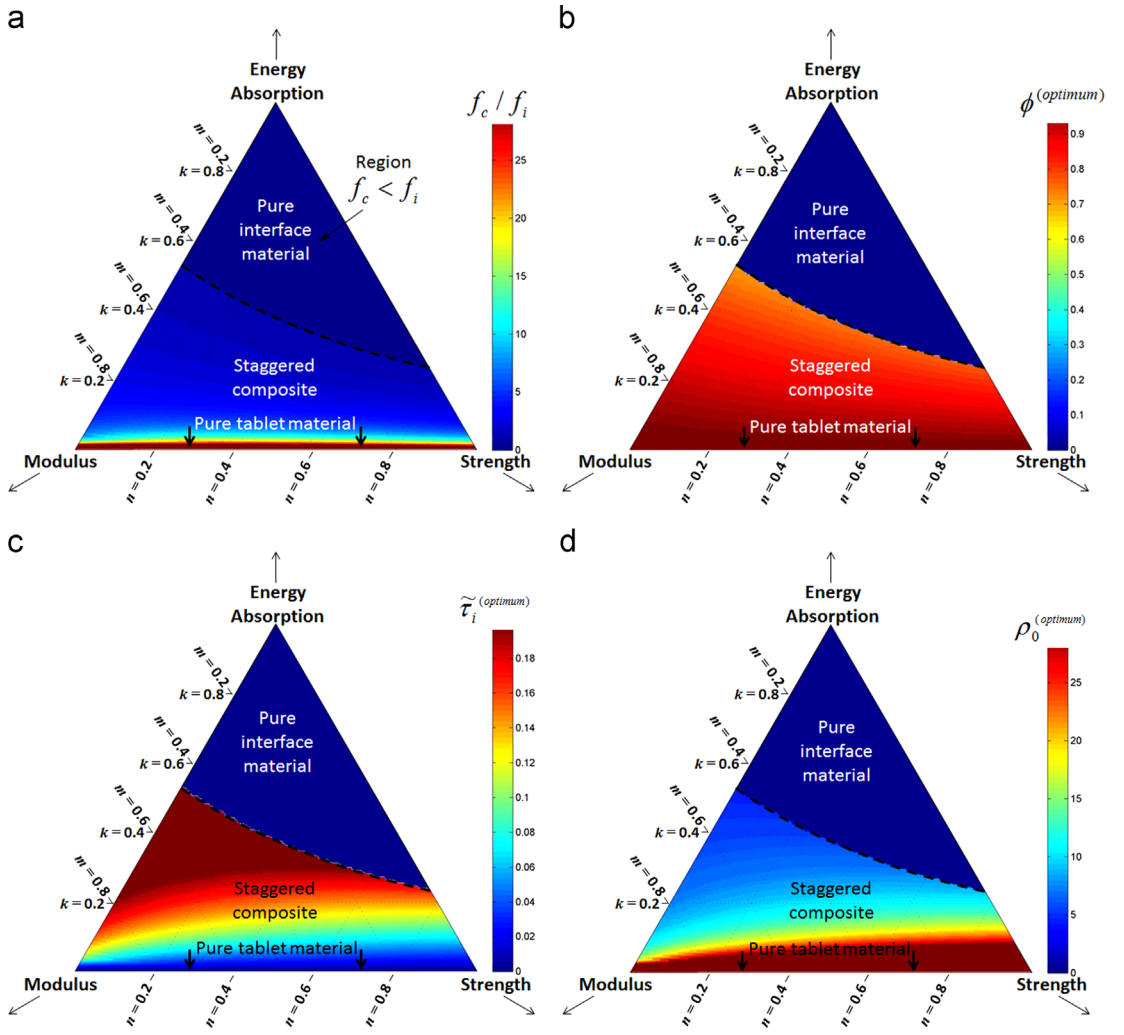

Fig. 8. Ternary diagrams showing optimum materials, composition and microstructure for all combinations (m,n,k), $a/t_t = 0.1$ and $\tilde{E}_i = \tilde{\tau}_i$. The optimum failure criterion was used. (a) fitness of the composite normalized by the fitness of the pure interface material; (b) optimum tablet concentration; (c) optimum interface strength and (d) optimum overlap length.

left corner represents designs for which high modulus is desired (high m), the lower right corner represents designs for which high strength is desired (high n), and the upper corner represents designs for which high energy absorption is desired (high k). For $k=0$ all the emphasis is on strength and stiffness, and the pure tablet material is always the best design. For larger values of k, the staggered material becomes beneficial and optimum combinations of $\tilde{\tau}_i$ and ϕ can be calculated as function of (m,n,k). As more energy absorption is desired (index k increasing), ϕ must decrease, and $\tilde{\tau}_i$ increases. Beyond a certain threshold, $\tilde{\tau}_i$ becomes so high that the pure interface material is more advantageous that the staggered structure. The fitness of the pure interface material is written

$$f_i = \tilde{E}_i^{\,m} \tilde{\sigma}_i^{\,n} \tilde{U}_i^{\,k} \text{ with } \tilde{\sigma}_i = \sqrt{3}\tilde{\tau}_i \tag{29}$$

Fig. 8a shows the ternary diagram for the fitness of the composite material. The region in the upper half of the ternary diagram corresponds to $f_i > f_c$, and to cases where the pure interface material is more beneficial. This frontier can also be seen in the other ternary diagrams, and has two important implications: first, the staggered structure is only advantageous if a large volume of tablets ($\phi > 0.7$) is used (Fig. 8b). Second, the staggered structure is only advantageous if there is a relatively high contrast of strength between tablets and interfaces with $\tilde{\tau}_i < 0.2$, that is the strength of the interface should not exceed one fifth of the strength of the tablets (Fig. 8c). Finally Fig. 8d shows the optimum overlap ratio for the tablets which must decrease as more energy absorption is desired. The lower region of the ternary diagram also display very useful general design guidelines: if high modulus and high strength are desired over energy absorption then it is more advantageous to use low interface strength, and high concentration of tablets with high overlap ratios. On the other hand, if more energy dissipation is desired then the interface strength should be increased, and lower concentrations of tablets with smaller overlap ratios should be used.

Finally, we note that the overall distribution of optimum parameters is organized along horizontal layers (k=constant) on the ternary diagrams. This indicates that the optimum designs do not change significantly with m and n if k is fixed. Designs which are beneficial to high modulus are also beneficial to high strength. This trend is consistent with general trends in monolithic and composites materials: stiffness usually goes together with strength (Barthelat and Mirkhalaf, 2013; Ashby, 1999). Following this observation, we plot the properties of the optimum composites as function of tablet

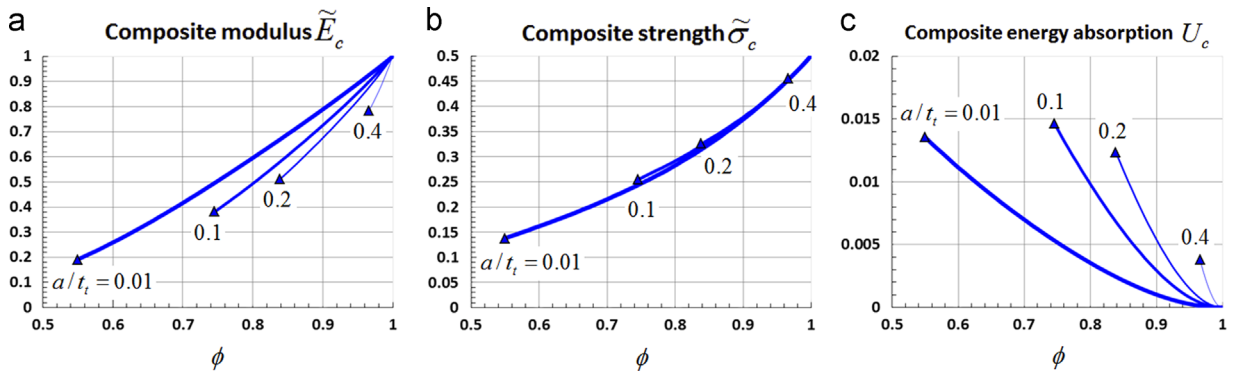

Fig. 9. Properties from optimum designs for energy absorption (low ϕ) or stiffness and strength (high ϕ): (a) modulus; (b): strength, (c): energy absorption. The triangular markers indicate the frontier between staggered structure and pure interface material.

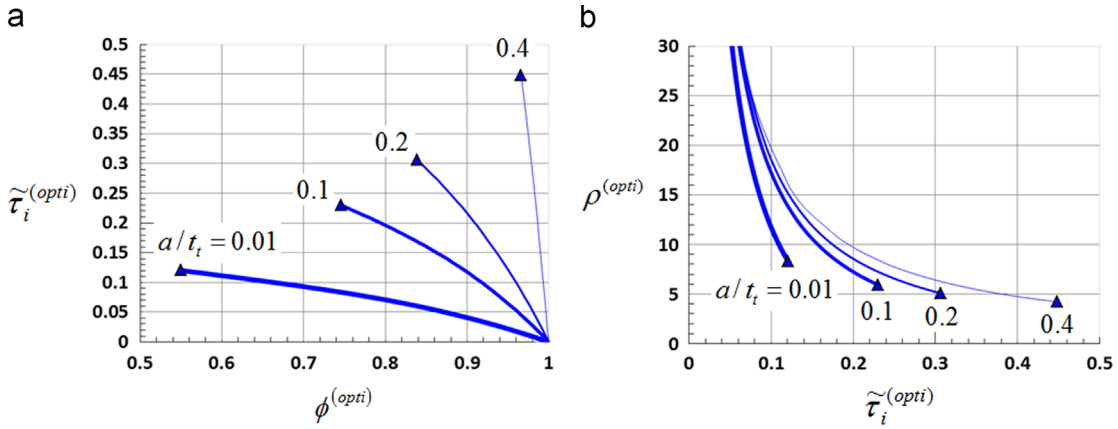

Fig. 10. Diagrams used to find optimum designs: (a) Optimum interface shear strength as function of tablet concentration and (b) Optimum overlap as function of interface shear strength. The curves are given for four different sizes of defects in the tablets.

concentration and along a vertical line in the ternary diagrams ($m=n$) on Fig. 9. As expected the optimum modulus and strength increase with ϕ (Fig. 9a and b) while the energy absorption decreases with ϕ (Fig. 9c). The triangular markers mark the frontier between staggered structure and pure interface material. These plots show that it is more difficult to efficiently implement the staggered structure if the tablets contain large defects (larger a/t_t). Note that the ternary diagrams and results on Figs. 8 and 9 were generated with $\kappa=0.25$, corresponding to the case of a random overlap length in the composite. Remarkably, we found that these results are virtually identical for other values of κ (within $0<\kappa\leq 0.5$).

7. Step-by-step optimization for staggered composites

We can now use these results to elaborate a step-by-step approach to the design and optimization of staggered composites. To aid this process we use Fig. 10a and b.

Step 1: Material selection for tablets: Choose the material and the size of the tablets: The modulus E_t must be high, so ceramics are good candidates. The tensile strength of the tablets should be maximized, which can be done by maximizing their toughness K_{IC} and/or minimizing the relative defect size a/t_t and/or minimizing their thickness t_t. Compute the tensile strength of the tablets in uniaxial tension using Eq. (5) $\sigma_t=\frac{K_{IC}}{f_0\sqrt{\pi a}}$.
Step 2: Volume concentration of tablets. Use Fig. 9 to select the appropriate tablet concentration ϕ which will generate the desired balance between modulus, strength and energy absorption for the composite. If large defects are present in the tablets, the energy absorption capabilities of the composite will decrease and ϕ should be as large as possible.
Step 3: Optimum interface strength. Use Fig. 10a and ϕ to determine the optimum interface shear strength $\tilde{\tau}_i^{(opti)}$.
Step 4: Material selection for the interfaces. Compute the actual desired shear strength of the material $\tau_i^{(opti)}=\sigma_t\tilde{\tau}_i^{(opti)}$. Select a material for the interfaces with the appropriate strength. The interface should also be highly extensible so that γ_i is maximized. Check that γ_i satisfies the optimum post-yield shear transfer condition (Eq. (19)). If that condition cannot be met, consider decreasing ϕ and return to step 1.
Step 5: Optimum overlap: Use Fig. 10b and $\tilde{\tau}_i^{(opti)}$ to determine the optimum overlap ${\rho_0}^{(opti)}$. Alternatively, ${\rho_0}^{(opti)}$ may be computed using Eq. (27a). Use Eq. (4) to compute the aspect ratio of the tablet $\rho^{(opti)}$.

8. Example: the design of nacre

We now illustrate these guidelines with natural nacre. Step 1 is the selection of the material and properties of the tablets. The tablets are made of calcium carbonate (aragonite) and their thickness is $t_t\approx 500$ nm. The size of the defects is not known, and we assume that they are in the order of the size of the nanograins the tablets are made of ($a=50$ nm). This gives $a/t_t=0.1$. Using $K_{IC}=0.4$ MPa .m$^{1/2}$ for calcite (Broz et al., 2006) gives a tensile strength of $\sigma_t\approx 900$ MPa for the tablets in *uniform tension* (not within the staggered structure). Step 2 focuses on determining the concentration of the tablets. In Fig. 10 we note that for $a/t_t=0.1$ the volume concentration of the tablets must be at least 0.75. We choose $\phi=0.95$, which is the values for nacre, and which gives a combination of high modulus, high strength with some energy absorption. We then move on step 3 and Fig. 10a, which give the optimum shear strength for the interface. For $a/t_t=0.1$ and $\phi=0.95$ we get $\tilde{\tau}_i^{(opti)}=0.06$. Step 4 examines the actual optimum properties of the interfaces. Here the optimum shear strength is $\tau_i^{(opti)}=\sigma_t\times\tilde{\tau}_i^{(opti)}=54$ MPa which is remarkably close to the actual shear strength of the interfaces in nacre (Barthelat et al., 2007). Finally, in step 5 we determine the optimum aspect ratio of $\rho^{(opti)}\approx 30$, which is higher than the actual aspect ratio of the tablets in nacre from red abalone ($\rho\approx 13$) but within the same magnitude. A large unknown in the procedure is the size of the defect in the tablets. Using $a/t_t=0.2$ and $\varphi=0.95$ would give we get $\tau_i^{(opti)}\approx 100$ MPa and $\rho^{(opti)}\approx 15$. The predictions from the optimization method are quite close to the actual value for nacre, considering that the only starting point for the procedure is the tablet properties and volume concentration.

9. Summary and discussion

In this article we have incorporated basic mechanical models into an optimization scheme for the design of staggered composites, for any desired combination of stiffness, strength and energy absorption. We have incorporated the material properties for tablets and matrix as optimization variables and not simple inputs. As opposed to previous models we also considered cases where the tablets do not fully overlap, with particular attention to the case $\kappa=0.25$ which corresponds to the case where the overlap between tablets is random. Most of the previous approaches on optimizing staggered structures have examined the effect of microstructure or hierarchy on each property, without solving some of the design contradictions associated to this problem. Here we have, for the first time, addressed this issue by using a fully tunable multi-objective optimization scheme to maximize stiffness, strength and energy absorption simultaneously. In addition, all of the precious approaches to design optimization have assumed fixed properties for the tablets and interfaces. Here we have incorporated these properties as design variables, leading to a more comprehensive optimization approach and more efficient designs. The models used here to predict basic properties for the composite are very simple but provide good estimates, in reasonable agreement with experiments. Using more sophisticated models which would include the effect of gaps and

matrix materials at the ends of the tablets, three dimensionality (Barthelat et al., 2007; Katti et al., 2001), effect of tablet arrangement (Rabiei et al., 2010; Zhang et al., 2010) stochastic microstructure, rough (Evans et al., 2001) and/or wavy tablets (Barthelat et al., 2007), relaxation of the $\tilde{E}_i \approx \tilde{\tau}_i$ assumption and multi-axial loading would certainly lead to more refined optimized designs. Nevertheless, useful general guidelines emerge from the present work: the staggered microstructure is only advantageous if the tablets are at least 5 times stronger than the interfaces, and only if high volume concentrations of tablets are used. Remarkably, we found that these results are virtually identical for any value of the overlap ratio κ (within $0 < \kappa \leq 0.5$). The exact trends produced by the optimization process were compiled in a step-by-step optimization process which produces results which are consistent with the materials and microstructure of natural nacre. The method is general and can be applied to any other set of materials. The method also incorporates size effects through fracture mechanics of the tablets, and is therefore appropriate to the design and optimization of micro- and nano-composites. Tablets or inclusions with sizes approaching nanometers can be much stronger than microtablets, which enables larger aspect ratio and higher performances. However, it is difficult to achieve high volume concentrations of tablets for nanostructured composites, because their optimum design would imply interfaces of sub-nanometer thickness. Finally, the advantages of structural hierarchy in composite were highlighted in recent model (Gao, 2006; Zhang et al., 2011; Sen and Buehler, 2011). Implementing this systematic design approach to multi-scale staggered structures may yield interesting guidelines for the optimization of modern composite materials.

References

Adams, R.D., Peppiatt, N.A., 1974. Stress analysis of adhesive-bonded lap joints. J. Strain Anal. Eng. Des. 9, 185–196.

Ashby, M.F., Materials Selection and Process in Mechanical Design, ed. B. Heinemann1999, Oxford.

Bar-On, B., Wagner, H.D., 2011. Mechanical model for staggered bio-structure. J. Mech. Phys. Solids 59 (9), 1685–1701.

Bar-On, B., Wagner, H.D., 2013. New insights into the Young's modulus of staggered biological composites. Mater. Sci. Eng. C-Mater. Biol. Appl. 33 (2), 603–607.

Bar-On, B., Wagner, H.D., 2013. Structural motifs and elastic properties of hierarchical biological tissues—A review. J. Struct. Biol. 183 (2), 149–164.

Barthelat, F., 2007. Biomimetics for next generation materials. Philosophical Trans. R. Soc. Math. Phys. Eng. Sci. 365, 2907–2919.

Barthelat, F., Mirkhalaf, M., 2013. The quest for stiff, strong and tough hybrid materials: an exhaustive exploration. J. R. Soc. Int 10 (89). http://dx.doi.org/10.1098/rsif.2013.0711. (Article no. 20130711).

Barthelat, F., Rabiei, R., 2011. Toughness amplification in natural composites. J. the Mech. Phys Solids 59 (4), 829–840.

Barthelat, F., Zhu, D.J., 2011. A novel biomimetic material duplicating the structure and mechanics of natural nacre. J. Mater. Res. 26 (10), 1203–1215.

Barthelat, F., et al., 2006. Mechanical properties of nacre constituents and their impact on mechanical performance. J. Mater. Res. 21 (8), 1977–1986.

Barthelat, F., et al., 2007. On the mechanics of mother-of-pearl: a key feature in the material hierarchical structure. J. Mech. Phys. Solids 55 (2), 225–444.

Barthelat, F., Dastjerdi, A.K., Rabiei, R., 2013. An improved failure criterion for biological and engineered staggered composites. J. R. Soc. Interface 10, 79.

Begley, M.R., et al., 2012. Micromechanical models to guide the development of synthetic 'brick and mortar' composites. J. Mech. Phys. Solids 60 (8), 1545–1560.

Bekah, S., Rabiei, R., Barthelat, F., 2011. Structure, scaling, and performance of natural micro- and nanocomposites. Bionanoscience 1 (1), 53–61.

Bonderer, L.J., Studart, A.R., Gauckler, L.J., 2008. Bioinspired design and assembly of platelet reinforced polymer films. Science 319 (5866), 1069–1073.

Broz, M.E., Cook, R.F., Whitney, D.L., 2006. Microhardness, toughness, and modulus of Mohs scale minerals. Am. Mineral. 91 (1), 135–142.

Chen, B., Wu, P.D., Gao, H., 2009. A characteristic length for stress transfer in the nanostructure of biological composites. Compos. Sci. Technol. 69 (7–8), 1160–1164.

Currey, J.D., 1977. Mechanical properties of mother of pearl in tension. Proc. R. Soc. Lond. 196 (1125), 443–463.

Dimas, L.S., et al., 2013. Tough Composites inspired by mineralized natural materials: computation, 3d printing, and testing. Adv. Fun. Mater. 23 (36), 4629–4638.

Espinosa, H.D., et al., 2009. Merger of structure and material in nacre and bone—Perspectives on de novo biomimetic materials. Prog. Mater. Sci. 54 (8), 1059–1100.

Evans, A.G., et al., 2001. Model for the robust mechanical behavior of nacre. J. Mater. Res. 16 (9), 2475–2484.

Fernandes, A.N., et al., 2011. Nanostructure of cellulose microfibrils in spruce wood. Proc. Ntl. Acad. Sci. USA 108 (47), E1195–E1203.

Fratzl, P., Weinkamer, R., 2007. Nature's hierarchical materials. Prog. Mater. Sci. 52 (8), 1263–1334.

Gao, H.J., 2006. Application of fracture mechanics concepts to hierarchical biomechanics of bone and bone-like materials. Int. J. Fract. 138 (1–4), 101–137.

Gao, H.J., et al., 2003. Materials become insensitive to flaws at nanoscale: Lessons from nature. Proc. Ntl. Acad. Sci. USA 100 (10), 5597–5600.

Gosline, J.M., et al., 1999. The mechanical design of spider silks: from fibroin sequence to mechanical function. J. Exp. Biol. 202 (23), 3295–3303.

Guo, X. and H. Gao, 2006. Bio-inspired material design and optimization. In: Proceedings of the IUTAM Symposium on Topological Design Optimization of Structures, Machines and Materials: Status and Perspectives, ed. M.P. Bendsoe, N. Olhoff, O. Sigmund. vol. 137. 439–453.

Gupta, H.S., et al., 2005. Nanoscale deformation mechanisms in bone. Nano Lett. 5 (10), 2108–2111.

He, L.H., Swain, M.V., 2008. Understanding the mechanical behaviour of human enamel from its structural and compositional characteristics. J. Mech. Behav. Biomed. Mater. 1 (1), 18–29.

Jackson, A.P., Vincent, J.F.V., Turner, R.M., 1988. Mech. Des. Nacre. Proc. R. Soc. Lond. 234 (1277), 415–440.

Jager, I., Fratzl, P., 2000. Mineralized collagen fibrils: a mechanical model with a staggered arrangement of mineral particles. Biophys. J. 79 (4), 1737–1746.

Katti, D.R., et al., 2001. 3D finite element modeling of mechanical response in nacre-based hybrid nanocomposites. Comput. Theor. Polym. Sci. 11, 397–404.

Keten, S., et al., 2010. Nanoconfinement controls stiffness, strength and mechanical toughness of beta-sheet crystals in silk. Nat. Mater. 9(4): p. 359–367.

Kotha, S.P., Li, Y., Guzelsu, N., 2001. Micromechanical model of nacre tested in tension. J. Mater. Sci. 36 (8), 2001–2007.

Lei, H.J., et al., 2013. Elastic bounds of bioinspired nanocomposites. J. Appl. Mech. Trans. Asme 80, 6.

Liu, B., Zhang, L., Gao, H., 2006. Poisson ratio can play a crucial role in mechanical properties of biocomposites. Mech. Mater. 38 (12), 1128–1142.

Luz, G.M., Mano, J.F., 2009. Biomimetic design of materials and biomaterials inspired by the structure of nacre. Philos. Trans. R. Soc. –Math. Phys. Eng. Sci. 367 (1893), 1587–1605.

Marler, R.T., Arora, J.S., 2004. Survey of multi-objective optimization methods for engineering. Structural and Multidisciplinary Optimization, Vol. 26. Springer.

Mayer, G., 2005. Rigid Biological Systems as Models for Synthetic Composites Science, 310(5751). 1144–1147.

Meyers, M.A., et al., 2008. Biological materials: structure and mechanical properties. Prog. Mater. Sci. 53, 1–206.

Okumura, K., de Gennes, P.G., 2001. Why is nacre strong? Elastic theory and fracture mechanics for biocomposites with stratified structures. Eur. Phys. J. E 4 (1), 121–127.

Ortiz, C., Boyce, M.C., 2008. Materials science—Bioinspired structural materials. Science 319 (5866), 1053–1054.

Rabiei, R., Bekah, S., Barthelat, F., 2010. Failure mode transition in nacre and bone-like materials. Acta Biomater. 6, 4081–4089.

Rabiei, R., Bekah, S., Barthelat, F., 2012. Nacre from mollusk shells: inspiration for high performance nanocomposites. In: John, M.J., Thomas, S. (Eds.), Natural Polymers, Volume II: Natural Polymer Nanocomposites. Royal Society of Chemistry.
Rousseau, M., et al., 2005. Multiscale structure of sheet nacre. Biomaterials 26 (31), 6254–6262.
Sen, D., Buehler, M.J., 2011. Structural hierarchies define toughness and defect-tolerance despite simple and mechanically inferior brittle building blocks. Sci. Rep., 1.
Shao, Y., et al., 2012. Discontinuous crack-bridging model for fracture toughness analysis of nacre. J. Mech. Phys. Solids 60 (8), 1400–1419.
Shrivastava, S.C., Jonas, J.J., Canova, G., 1982. Equivalent strain in large deformation torsion testing—Theoretical and practical considerations. J. Mech. Phys. Solids 30 (1–2), 75–90.
Smith, B.L., et al., 1999. Molecular mechanistic origin of the toughness of natural adhesives, fibres and composites. Nature (London) 399 (6738), 761–763.
Tada, H., Paris, P.C., Irwin, G.R., 2000. The Stress Analysis of Cracks Handbook, Third Edition ed, ed A. press.
Vendrasco, M.J., Checa, A.G., Kouchinsky, A.V., 2011. Shell microstructure of the early bivalve pojetaia and the independent origin of nacre within the mollusca. Palaeontology 54, 825–850.
Volkersen, O., 1938. Die Nietkraftverteilung in zugbeanspruchten Nietverbindungen mit konstanten Laschen-guerschnitten. Luftfahrtforschung 15, 41–47.
Wang, R.Z., et al., 2001. Deformation mechanisms in nacre. J. Mater. Res. 16, 2485–2493.
Wegst, U.G.K., et al., 2010. Biomaterials by freeze casting. Philos. Trans. R. Soc. Math. Phys. Eng. Sci. 368 (1917), 2099–2121.
Wei, X.D., Naraghi, M., Espinosa, H.D., 2012. Optimal length scales emerging from shear load transfer in natural materials: application to carbon-based nanocomposite design. Acs Nano 6 (3), 2333–2344.
Yourdkhani, M., Pasini, D., Barthelat, F., 2011. Multiscale mechanics and optimization of gastropod shells. J. Bionic Eng. 8 (4), 357–368.
Zhang, Z., Zhang, Y.-W., Gao, H., 2011. On optimal hierarchy of load-bearing biological materials. Proc. R. Soc. B-Biol. Sci. 278 (1705), 519–525.
Zhang, Z.Q., et al., 2010. Mechanical properties of unidirectional nanocomposites with non-uniformly or randomly staggered platelet distribution. J. Mech. Phys. Solids 58 (10), 1646–1660.